*Science in China*: *Series D Earth Sciences* 2006 Vol.49 No.2 124—132

**DOI: 10.1007/s11430-004-5220-3**

# Characteristics and quantitative of negative ion in salt aqueous solution by Raman spectroscopy at –170℃

ZHANG Nai, ZHANG Dajiang, ZHANG Shuichang & ZHANG Dijia

Research Institute of Petroleum Exploration and Department, Key Laboratory of Petroleum Geochemistry and Key Laboratory for Oil and Gas Reservoirs, CNPC, Beijing 100083, China
Correspondence should be addressed to Zhang Nai (email:naizhang@vip.sina.com)

Received June 5, 2004; accepted May 26, 2005

**Abstract** The results from Raman spectroscopy analysis of salt aqueous solutions at –170℃ demonstrate that for those clearly sharp iron peaks whose Raman wavenumber is close to each other such as $NO_3^-$ and $CO_3^{2-}$, their original shape could be restorable by the stripping technique, and that ice's sharp characteristic peak (3090—3109 $cm^{-1}$) is steady, while the spectrum band of the complex compound ($nCl^-—[H^+—OH^-]_n$) chlorine ion combined chemically with water molecule is 3401—3413 $cm^{-1}$. On the other hand, the research shows that the higher the negative iron concentration, the stronger its Raman characteristic peak intensity and the smaller the ice's. Based on the number of data and theoretical work, the strong correlation of the molar concentration of negative ion with the $S_i/S_{H_2O}$ band area ratio is built up. Moreover, the developed Raman method is successfully used in the component analysis of the field fluid inclusions from Silurian sandstone in Tarim basin.

**Keywords: Raman, negative ion, complex compound $nCl^-—[H^+—OH^-]_n$, concentration, Tarim basin.**

The salinity of fluid inclusions is an important parameter, which gives scientists the ability to understand paleo-fluid chemistry, the forming of deposit and petroleum as well as the evolution in geological history[1]. Generally, the parameter is estimated to roughly represent the natural frame of geological fluid using the ice melting temperature and first melting temperature from microthermometry apparatus, because fluid inclusion is so small (＜100 μm in size) that the fluid in inclusion is difficult to be extracted for the bulk composition analysis[2–9]. Therefore, more reliable information on the salinity of fluid inclusion has attracted the scientists' attention.

As a nondestructive analysis tool, the Raman technique has been applied to the measurement of single inclusion[10,11] and the identification of negative ions in fluid inclusions such as $CO_3^{2-}$, $HCO_3^-$, $SO_4^{2-}$ and $NO_3^-$. But the performance depends on whether the experiments could solve a series of common problems or not, including the recognition of the close Raman peaks, for example, $NO_3^-$ and $CO_3^{2-}$ [12], and of single element negative ion such as $Cl^-$, which usually cannot be seen in Raman spectra[13]. Another problem is that as a necessary carrier of geological fluid, water at room temperature displays such a large and intense envelope in Raman spectrogram that either its intensity cannot be precisely ascertained[14—16], or other

important information is concealed.

In this research, a range of controlled experiments at −170℃ make the Raman characteristic peak, such as $n\mathrm{Cl}^-$—$[\mathrm{H}^+$—$\mathrm{OH}^-]_n$, negative ions in mixed solution and the ice (3090—3108 $\mathrm{cm}^{-1}$) clearly visible, and the regularity that the negative ion intensity strengthen and the ice intensity weaken with the increasing ions molar concentration ruled out and the curve graph which expose a positive correlation between the $S_i / S_{\mathrm{H_2O}}$ band area ratio and the negative ion molar concentration built up. Finally, a field application arising from the knowledge of qualitative and quantitative spectrometric analysis of negative ions and the bulk salinity of fluid inclusion in diagenetic cements from Silurian sandstone in the Tarim Basin provides a detailed record of the paleo-fluid evolution and proves that the Raman spectra method at −170℃ is very effective in working out the evolution of the unknown geological fluid.

## 1 Experiments

### *1.1 Samples*

Series of standard aqueous solution (GB652-GB672), including chlorate $\mathrm{Cl}^-$, sulfate $\mathrm{SO_4^{2-}}$, nitrate $\mathrm{NO_3^-}$, carbonate $\mathrm{CO_3^{2-}}$, bicarbonate $\mathrm{HCO_3^-}$ and different sorts of negative ion population solution, *etc*. with all kinds of positive ions ($\mathrm{Na}^+$, $\mathrm{K}^+$, $\mathrm{Ca}^{2+}$, $\mathrm{Mg}^{2+}$, $\mathrm{Cu}^{2+}$, $\mathrm{Mn}^{2+}$, $\mathrm{Fe}^{3+}$), are prepared by Laboratory Center, RIPED in China, according to the composition of natural fluid inclusion[5,9,17]. A total of 769 experiments sample have been done.

### *1.2 Instrument*

Raman spectral characterization of samples was recorded on Raman spectrograph JY-1000 (made in France) ($\mathrm{Ar}^+$ laser 514.532 nm, laser power at the sample surface 2—4 mW, objective lens 50×LWD). The sample set in the freezing room of heating and freezing stage was tested at −170℃ for 30 s and the solution was sealed in the quartz crucible. The hole size was as follows: 300 μm at room temperature and 100 μm at −170℃ for solution, 1—5 μm for inclusion.

## 2 Results and discussion

### *2.1 Raman characteristics for individual negative-ion solution at –170 ℃*

Although the shape of the water band appears a broad profile at room condition[14−16]. the spectrums of the saline solutions at −170℃ have different patterns, notably in the presence of 3090—3109 $\mathrm{cm}^{-1}$, 3147—3229 $\mathrm{cm}^{-1}$ and 3262—3300 $\mathrm{cm}^{-1}$ (Fig. 1). Among them, the range of 3090—3109 $\mathrm{cm}^{-1}$ that is the ice characteristic peak with the reference of the previously published example is great sharp and steady so that its location and identity can be easily and precisely ascertained[18, 19].

Likewise, the sharp and stable band of the negative ions ($\mathrm{SO_4^{2-}}$, $\mathrm{NO_3^-}$, $\mathrm{CO_3^{2-}}$ and $\mathrm{HCO_3^-}$) appears to be characteristic at −170℃ besides the pinnacle of ice band. Because the ions have a good Raman activity as confirmed earlier, they are impossibly combined with the water molecule (Fig. 1). Under the same testing condition, as the concentration of negative ions is increased, their Raman spectra intensity become larger, such as $\mathrm{I}_{1046-1050}$ ($\mathrm{NO_3^-}$) and $\mathrm{I}_{1069}$ ($\mathrm{CO_3^{2-}}$)(Fig. 2), whereas the ice's ($\mathrm{I}_{3102-3109}$) become smaller.

Notice in Figs. 1, 3 that the spectrogram of chlorate solution with different positive ions is of a remarkable characteristic at −170℃. As a monovalent negative ion, $\mathrm{Cl}^-$ is so labile that it combines with water molecule [$\mathrm{H}^+$–$\mathrm{OH}^-$] to form a stable complex compound ($n\mathrm{Cl}^-$—$[\mathrm{H}^+$—$\mathrm{OH}^-]_n$), which exhibits a characteristic peak in Raman spectra. That is the reason why two sharp peaks (3401—3413 $\mathrm{cm}^{-1}$ and 3424—3438 $\mathrm{cm}^{-1}$) usually appear in the range of 3403—3440 $\mathrm{cm}^{-1}$ besides the ice peak in the spectrogram of chlorate solution. But the pattern has no presence in other kind of saline solution, for instant, sulfate $\mathrm{SO_4^{2-}}$ and carbonate $\mathrm{CO_3^{2-}}$ (Figs. 1 and 3).

Similarly, in the $\mathrm{H_2O}$-NaCl system, with the increasing concentration of negative ion, the Raman spectra intensity becomes larger, whereas the intensity

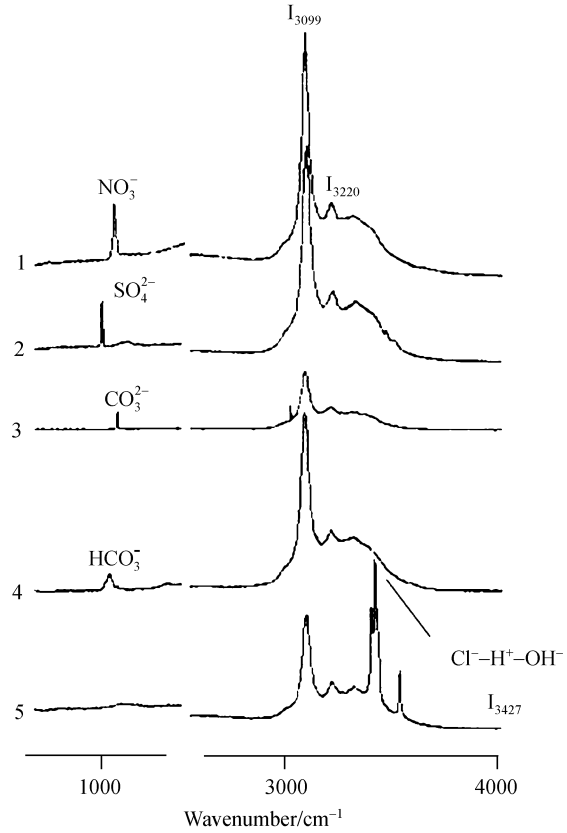


Fig. 1. Raman spectra of different $H_2O$-salt systems at −170℃. 1, $NaNO_3$ solution; 2, $Na_2SO_4$ solution; 3, $Na_2CO_3$ solution; 4, $NaHCO_3$ solution; 5, NaCl solution.

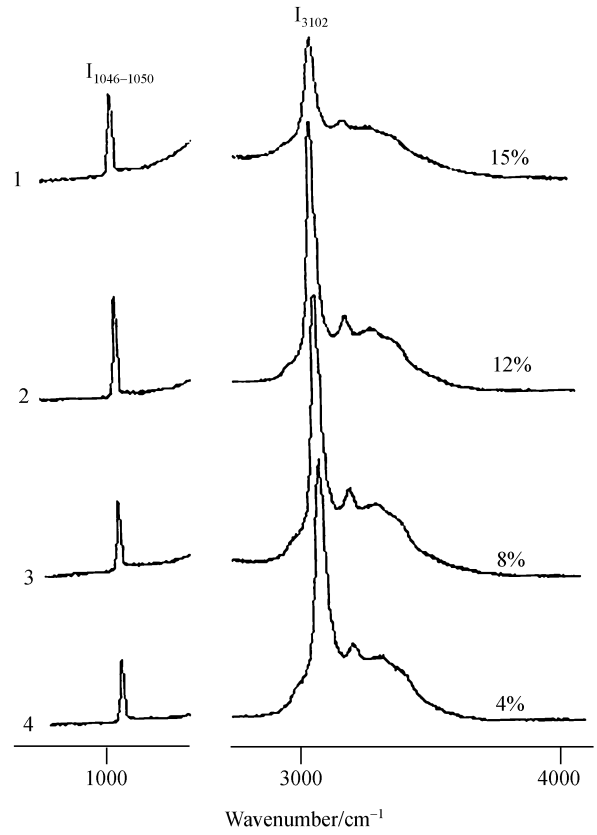


Fig. 2. Raman spectra of $H_2O$-$Ca(NO_3)_2$ systems with different concentration at −170℃.

of ice ($I_{3108}$) becomes smaller. The same change happens in the Raman spectra of other chlorate solutions, such as $CaCl_2$, $FeCl_3$, KCl, $CuCl_2$ and $NH_4Cl$ (Fig. 3(a), (b)). In brief, a positive correlation exists between Raman peak intensity of the negative ions and the concentration of those ions.

### *2.2 Raman characteristic for multi-negative ion solution at –170 ℃*

In the previous section, it is demonstrated that not only the negative ions and the ice in the single salt solutions respectively have their own distinct Raman peak, but the high correlation between the Raman peak intensity of the negative ion and the salinity of the single salt solution exists at −170℃. However, the geological fluid actually is diverse and usually consists of one more negative ion species. Whether these negative ion peaks, especially the adjacent peaks such as $NO_3^-$ and $CO_3^{2-}$, are themselves or transferred to others, needs to be carefully assessed. The experiment at −170℃ tests two-group solutions. One solution is composed of two kinds of salts and the other three kinds of salts.

Beginning with the double negative ions solution comprising sodium carbonate $Na_2CO_3$ and sodium nitrate $NaNO_3$, the examination shows that the $NO_3^-$ Raman spectra situation (1049.8 $cm^{-1}$ and 1048.3 $cm^{-1}$) is constant with those (1046－1050 $cm^{-1}$) from its pure solution and the $CO_3^{2-}$ wavenumber (1063.9 $cm^{-1}$, 1062.3 $cm^{-1}$) is only less than those (1069 $cm^{-1}$) from its pure solution. What's more, the overlapping peaks are restorable using the stripping technique in automatic or manual way. If only improving the $NaNO_3$ mole concentration of the solution, the intensity of $NO_3^-$ in Raman spectra will become stronger, whereas those of $CO_3^{2-}$ have no change (Fig. 4).

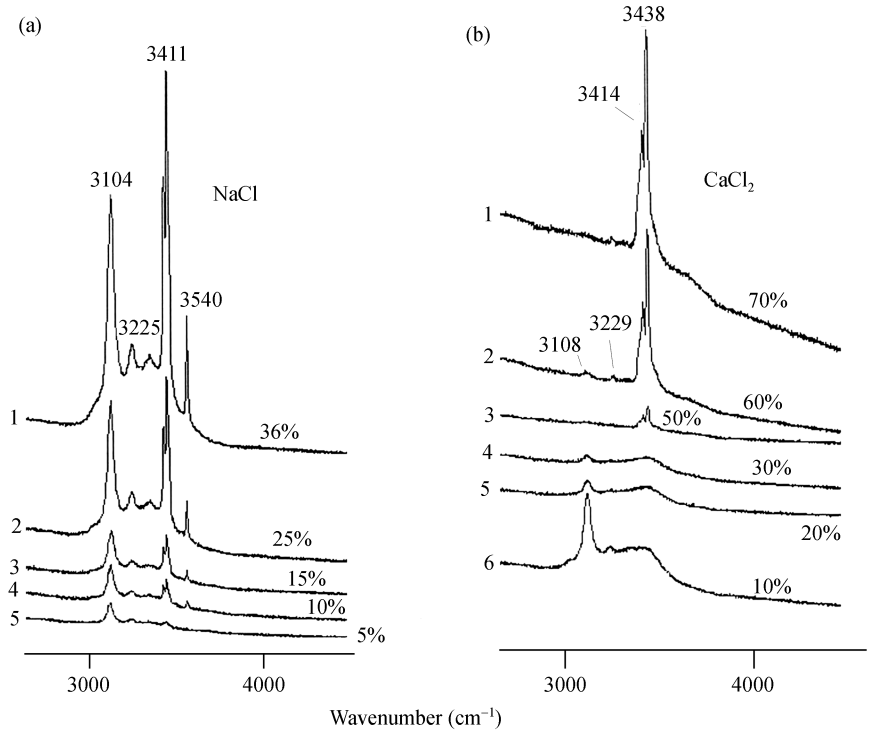


Fig. 3. Raman spectra of chlorate solution with different concentrations at −170℃.

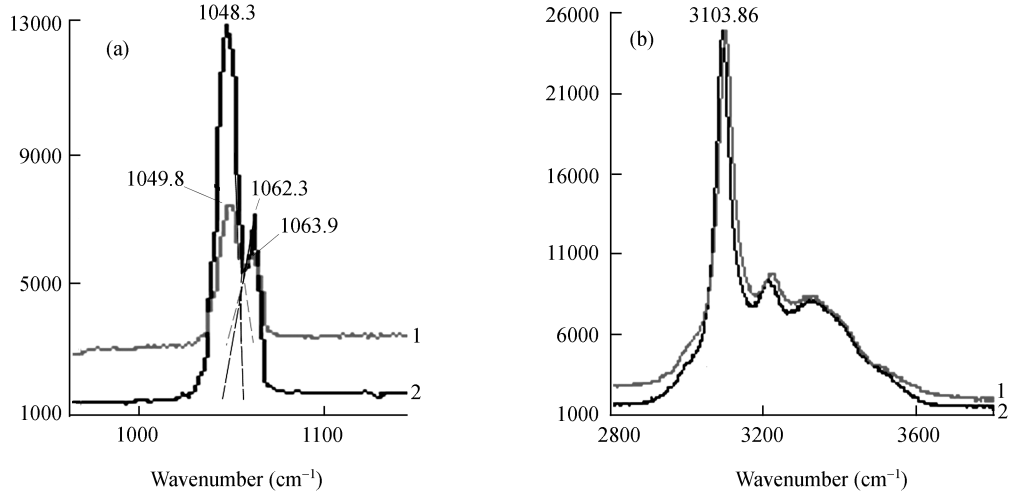


Fig. 4. Raman spectra of $H_2O$-$NaNO_3$-$Na_2CO_3$ systems with different concentrations at −170℃. 1, 5 g $NaNO_3$ and 5 g $Na_2CO_3$ dissolved in 100 g water. 2, 2.5 g $NaNO_3$ and 5 g $Na_2CO_3$ dissolved in 100 g water.

The second group solutions both contain three kinds of negative ions, which are sodium sulfate $Na_2SO_4$, sodium carbonate $Na_2CO_3$ and sodium nitrate $NaNO_3$. Each negative ion concentration in the solution named "a", is twice than those in the solution named "b". Obviously, the Raman spectra characteristic of the negative ions are the same as the related examples mentioned previously. Compared with the situation of the "b" solution, the negative ions peak's intensity in "a" solution markedly increases in uniform scale, confirming that the intensity depends on the ion concentration. Meanwhile, the ice peak intensity in "a" solution is still weaker than those of "b" solution because of the higher salinity in "a" solution (Fig. 5).

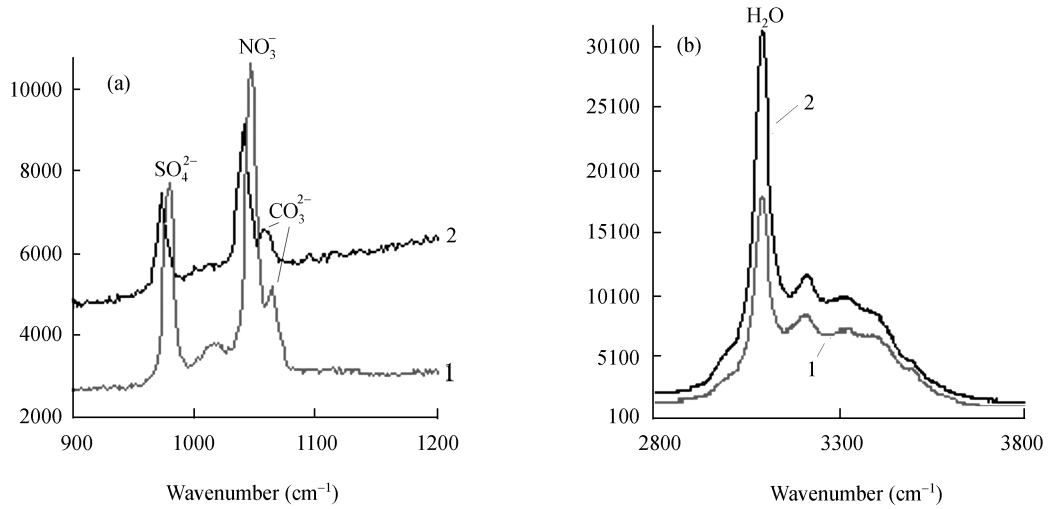


Fig. 5. Raman spectra of $H_2O-NaNO_3-Na_2CO_3-Na_2SO_4$ systems with different concentrations at −170℃. 1, 4 g $NaNO_3$, 4 g $Na_2CO_3$ and 4 g $Na_2SO_4$ dissolved in 100 g water. 2, 2 g $NaNO_3$, 2 g $Na_2CO_3$ and 2 g $Na_2SO_4$ dissolved in 100 g water.

### *2.3 Semi-quantitative analysis of the negative ion concentration at –170 ℃*

The Raman peak intensity ($I$) of a matter is positive correlation to the number of its molecule that contributes to the scattering process, and thus the mole percentage ($X$) of the negative ions in fluid inclusions can be derived from the intensity of their characteristic Raman peak relative to that of water (ice) using the following equation:

$$X_i(\text{mol}\%) = (I_i / F_i) / \left( \sum_{j=1}^{n} I_j / F_j \right),$$

where $I_i$ is the peak amplitude of a liquid component ($i$) in a inclusion and $F_j$ is the Raman scattering cross section of this component[20]. Considering the effect of the molecular weight, laser power, temperature and instrument on the intensity of a Raman peak, we propose the area intensity ($S_i$) of the Raman peak to estimate $I_i/F_j$ of the liquid component $i$ in inclusions, and the value $S_i$ can be directly read out from the spectra.

Note that the intensity or the area of the any special salt ($i$) increases with the analysis time, the ratio of $I_i / I_{H_2O}$ and $S_i / S_{H_2O}$ changes a little (Table 1). In addition, a very clear link, the ratio of $I_i / I_{H_2O}$ or $S_i / S_{H_2O}$ increasing with the concentration rather than the time or others, is evident. The significant information from all experiments confirms that a model can be reasonably developed to derive the variation of ions salinity (Fig.6). Thus as a function of the negative ion concentration, the relative area of negative ion Raman peak to those of ice around 3104 $cm^{-1}$ is shown in Fig. 6, in which five common negative ions ($Cl^-$, $SO_4^{2-}$, $NO_3^-$, $CO_3^{2-}$ and $HCO_3^-$) are checked. According to the patter diagram, if we know the ion type and the area from the Raman spectra characteristic peak, the $S_i / S_{H_2O}$ band area ratio can be calculated to find out the negative ions concentration in unknown solution.

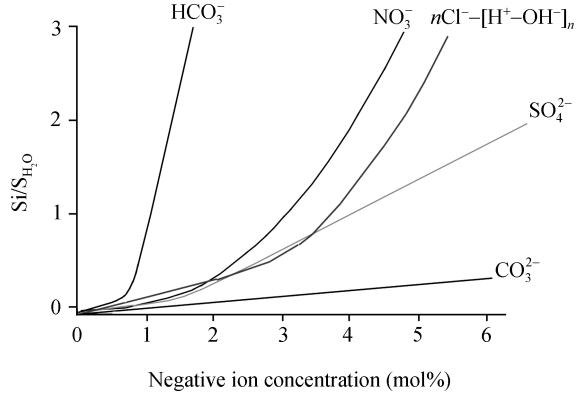


Fig. 6. The interrelated curve of the $S_i / S_{H_2O}$ Raman band area ratio with the negative ion concentration in fluid inclusion.

## 3 Application

According to the inclusion petrology feature, the growth sequence of diagenetic cements from Silurian

Table 1 Results of Raman spectroscopy analysis for the $H_2O$-NaCl system at −170℃

| Concentration(wt%) | Time (s) | $S_i$ | $S_{H_2O}$ | $S_i / S_{H_2O}$ | $I_i$(3147) | $I_{H_2O}$ | $I_i / I_{H_2O}$ |
|---|---|---|---|---|---|---|---|
| 10 | 5 | 3001 | 42153 | 0.071193 | 423 | 236 | 0.5579 |
| 10 | 10 | 5563 | 76092 | 0.073109 | 621 | 346 | 0.5572 |
| 10 | 20 | 10817 | 151132 | 0.071573 | 1207 | 673 | 0.5575 |
| 10 | 30 | 19962 | 275930 | 0.072344 | 1833 | 1019 | 0.5559 |
| 10 | 40 | 23307 | 328095 | 0.071037 | 2361 | 1321 | 0.5595 |
| 10 | 60 | 34140 | 468713 | 0.072838 | 2988 | 1665 | 0.5572 |

sandstone in the Tarim Basin is as follows: quartz growth of phase I (Fig. 7(a)), quartz growth of phase II (Fig. 7(b)), ferruginous dolomite (Fig. 7(c)), quartz cement (*i.e*. the cement in intergranular pore-space) (Fig. 7(d)), authigenic quartz (*i.e*. the crystal euhedron in pore space (Fig. 7(e)) and calcite cement (Fig. 7(f)). All the cements contain fluid inclusions.

As shown below, both the freezing method and Raman scattering technique are used in the fluid inclusion of the diagenetic cement in well TZ117. At first, the samples are cooled down to −170℃ in freezing room for the analysis of ion Raman spectrogram, and then heated to certain point to measure the parameters, namely the ice melting temperature and first melting temperature, which are commonly used to estimate the saline type and the salinity.

All data from samples in TZ117 (Table 2) have led to the realization that the freezing method can just provide geologists with the whole salinity and the rough saline composition about the geological fluid, which may be thought as an aqueous solution composed of one or two sorts of salt.

As seen from Table 2, the first melting temperature from the quartz overgrowth phase II and ferruginous dolomite is –27℃ and –24.3℃ respectively, and their ice melting temperature is –7.4℃ and –7.7℃. Consequently, the inclusions from different locations have approximately equal salinity of 11wt% so that the geological fluid is taken for a single kind of component halide solution.

However, based on Raman spectra (Figs. 8 and 9) and the model (Fig. 6), the molar concentration of negative ions can be determined by calculating the $S_i / S_{H_2O}$ band area ratio. The detailed data induce that during the quartz overgrowth phase II stage, the geological fluid is of high salinity with major carbonate and a lower amount of $Cl^-$, $SO_4^{2-}$, $HCO_3^-$, *etc*. (Fig. 9).

In short, the limited data from the freezing method show that the saline aqueous fluid from Silurian sandstone in the Tarim Basin only is chloride, whose salinity varies during the diagenetic evolution, whereas the evolution of the same geological fluid is classified into 4 stages with the help of the exactly qualitative and quantitative data using the Raman developed technique.

Four stages of the geological fluid are discussed as follows (Table 2):

1) In the first stage, the geological fluid which mainly contains chlorate with a little amount of sulfate and nitrate is of low salinity and quartz overgrowth of phase I is formed.

2) In second stage, the complex geological fluid is such a high saline solution predominantly composed of carbonates that quartz overgrowth of phase II and ferruginous dolomite is formed. There are a lot of inclusions in both kinds of the diagenetic cements.

3) And then, geological fluid with a lower salinity, which chiefly is chlorate, precipitates the clean quartz cement and later pure authigenic with a little of inclusions in pore space.

4) In the last stage, geological fluid is predominantly composed of carbonate with a high salinity so that a large number of calcite cements in which the inclusion salinity is as high as 22.2 mol% is formed.

In terms of the example above, it suggests that quartz could be generated in the geological fluid mainly composed of chloride (quartz I) or carbonate (quartz II), whereas the carbonate mineral (such as dolomite, calcite, *etc*.) is formed in the geological fluid that contains mainly carbonate. It also seems quite clear that the geological fluid comprising simple salt with lower salinity usually produces single pure min-

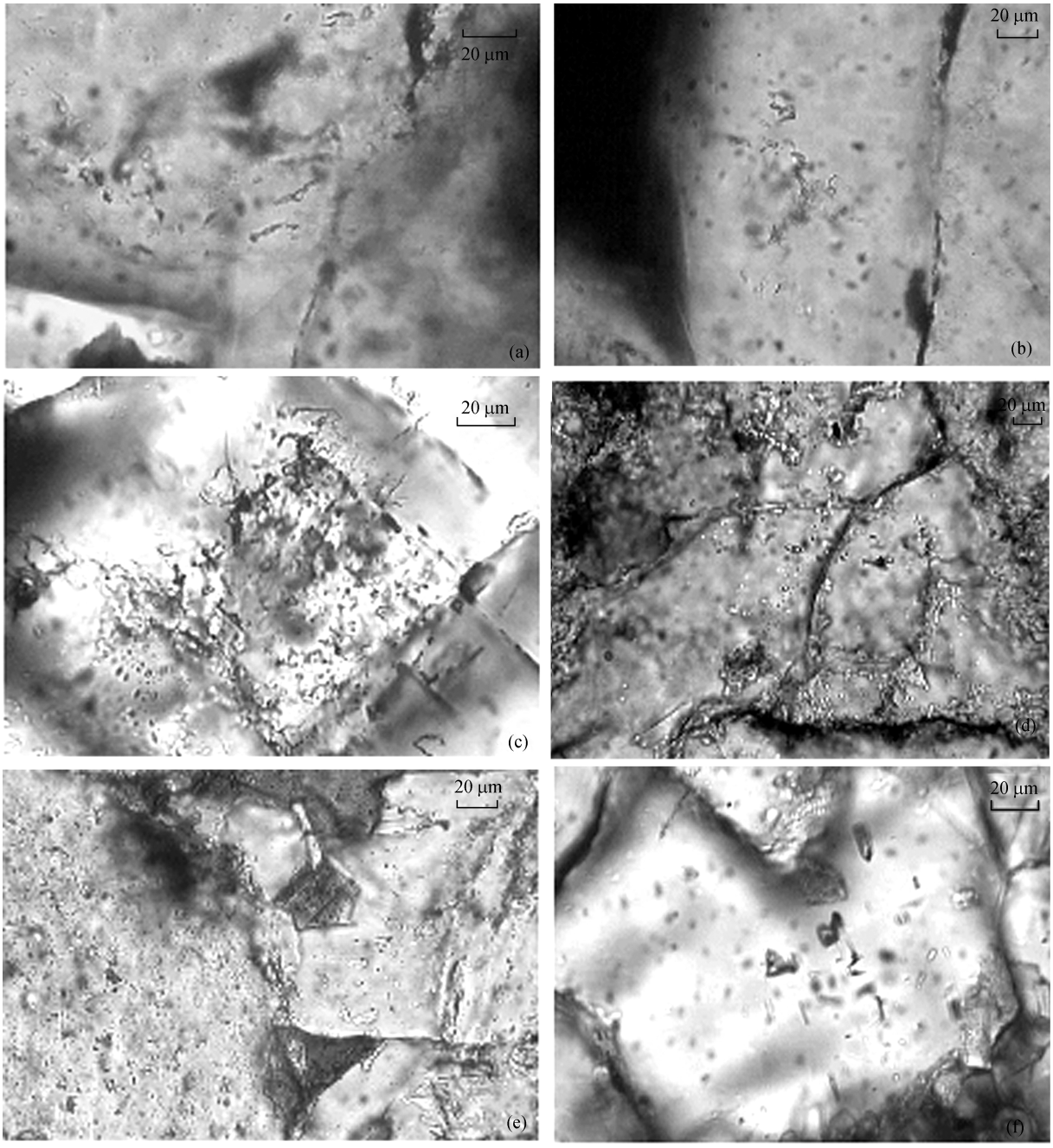


Fig. 7. Photomicrographs of the salt aqueous inclusions from Silurian sandstone in well TZ117. (a) the inclusion contained in quartz overgrowth I from sandstone , 4452 m. (b) the inclusion contained in quartz overgrowth II from sandstone , 4452 m. (c) the inclusion contained in ferruginous dolomite from the sandstone , 4433 m. (d) the inclusion contained in quartz cements from the sandstone , 4452 m. (e) the inclusion contained in authigenic quartz in pore space from the sandstone , 5592 m. (f) the inclusion contained in calcite cements from the sandstone , 4303 m.

eral, while the geological fluid comprising complex salts with high salinity might generally yield the multiple rock-forming minerals in which there are more impurity and inclusions.

## 4 Conclusions

A range of laboratory experiments prove that Raman spectra analysis of salt aqueous solution at –170℃ effectively eliminates the large and intense

Table 2 Parameters of fluid inclusions in disgenetic cements from Silurian sandstone in Tarim Basin

| Diagenetic cements | Freezing method | | | | | Raman scattering technique | | | | | | |
|---|---|---|---|---|---|---|---|---|---|---|---|---|
| | Sample number | $T_f$(℃) | $T_i$(℃) | Salts | Overall salinity (%) | Sample number | Negative ion concentration (mol %) | | | | | Overall salinity (%) |
| | | | | | | | $SO_4^{2-}$ | $CO_3^{2-}$ | $HCO_3^-$ | $NO_3^-$ | $Cl^-$ | |
| Quartz overgrowth of phase I | 2 | –18 | –1 | NaCl | 1.7 | 4 | 0.83 | 0 | 0 | 0.90 | 1.2 | 2.9 |
| Quartz overgrowth of phase II | 8 | –27 | –8 | NaBr | 11 | 8 | 2.4 | 12 | 0.82 | 0 | 4.5 | 20 |
| Ferruginous dolomite | 15 | –24 | –8 | NaCl | 11 | 5 | 1.7 | 5.1 | 0.83 | 2.3 | 1.8 | 12 |
| Quartz cement | 10 | –16 | –2 | NaCl KCl | 2.8 | 4 | 0.84 | 0 | 0 | 0 | 3.0 | 3.8 |
| Authigenic quartz | 0 | | | | | 1 | 1.0 | 1.0 | 0.21 | 0 | 1.5 | 3.7 |
| Calcite cement | 20 | –40 | –10 | $CaCl_2$ | 34 | 9 | 0.84 | 24 | 0.60 | 0 | 2.8 | 28 |

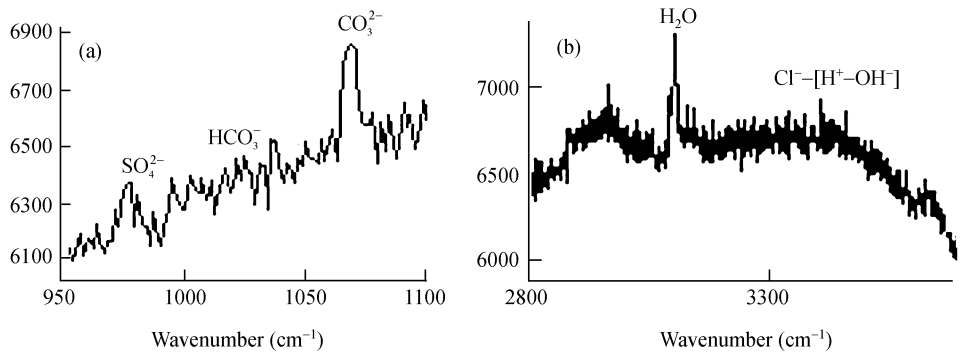


Fig. 8. Raman spectra of the salt aqueous inclusions from quartz overgrowth of phase II at –170℃.

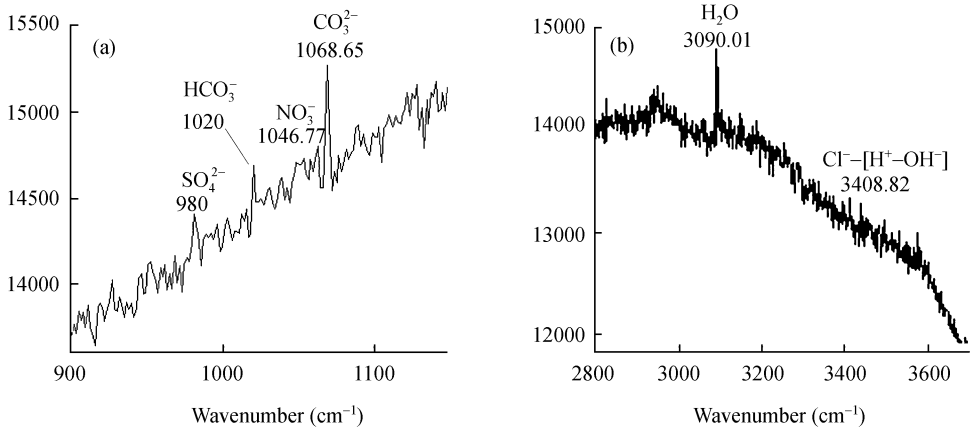


Fig. 9. Raman spectra of the salt aqueous inclusions from ferruginous dolomite at –170℃.

envelope of water compound band, and obviously displays the characteristic peak of $n\mathrm{Cl}^-—[\mathrm{H}^+—\mathrm{OH}^-]_n$ (*i.e.* 3411 $\mathrm{cm}^{-1}$). Additionally, the experiments show that a positive correlation exists between the $n\mathrm{Cl}^-—[\mathrm{H}^+—\mathrm{OH}^-]_n$ band intensity and the concentration of chloride solution. The higher the molar concentration of negative ion, the stronger the ion intensity and the smaller the ice's is. A number of data available from all kinds of experiments make it possible to build an interrelated curve of the $S_i / S_{\mathrm{H_2O}}$ band area ratio with the negative ion concentration, which can be used to derive the bulk composition of the negative ion in unknown geological fluid. Finally, a good example from Silurian sandstone in the Tarim Basin gives a quite powerful demonstration for the method. In other words, the developed Raman spectroscopy analysis method at $-170℃$ could identify the ions type and measure its molar concentration and the whole salinity in fluid inclusion, so the related research will help the geologists to obtain more scientific information on the evolution of geological fluid during diagenetic history.

## References


1. Roedder, E., Fluid inclusion, in Reviews in Mineralogy, Mineralogical Society of America, 1984, 12: 644.
2. Poty, Stalder, H. A., Weisbrod, A. M., Fluid incluision studies in quartz from fissures of the western and central Alps, Mineral, 1974, 54: 717－752.
3. Hollister, S., Techniques for analyzing fluid inclusions, Mineralogical Association of Canada, 1981, 272－277.
4. Ermakov, N. P., The study on mineralized solution, Kharlkov, Russian, 1950, 78－82.
5. Roedder, E., Technique for the extraction and partial chemical analysis of fluid-filled inclusions from minerals, Economic Geology, 1958, 3: 235－269.
6. Roedder, E., Studies of fluid inclusions I: Low temperature application of a double-purpose freezing and heating stage, Economic Geology, 1962, 7: 57.
7. Roedder, E., Fluid inclusion studies on the porphyry-type ore deposits at Bingham, Economic Geology, 1971, 1: 66.
8. Liu, B., Shen, K., Thermodynamics of Fluid Inclusions (in Chinese), Beijing: Geological Publishing House, 1999, 45.
9. Roedder, E., The composition of fluid inclusions, U.S. Geological Survey Professional Paper, 1972, 440-JJ: 164.
10. Brigite, W., Jill, D. P., John, J. F., Analysis of individual fluid inclusions by Fourier transform infrared and Raman microspectroscopy, Geochimica et Cosmochimica Acta, 1990, 54: 683－698.
11. Xu, P. C., Li, R. B., Raman Spectroscopy in Geosciences (in Chinese), Shanxi: Science Technology Publishing House, 1996, 78－122.
12. Burke, E. A., Raman microspectrometry of fluid inclusions, Lithos., 2001, 55: 139－158.
13. Dubessy, J., Gelsler, D., Kosztolanyi, C. *et al*., The Deyermination of Sulphate in Fluid Iinclusions Using the M.O.L.E. Raman Microprobe,Application to a Keuper Halite and Ggeochemical Cconsequences, Geochim. Cosmochim Acta, 1983, 47: 1－10.
14. Busing, W. R., Hornig, D., F., The effect of dissolved KBr KOH or HCl on the raman spectrum of water, Journal Chemical Physical, 1961, 65: 284－292.
15. Walrafen, G. E., Raman spectral studies of the effects of electrolytes on water, Journal Chemical Physical, 1962, 36: 1035－1042.
16. Walrafen, G. E., Raman spectral studies of water structure, Journal Chemical Physical, 1962, 40: 3249－3256.
17. He, Z. L., Inclusions Mineralogy (in Chinese), Beijing: Geological Publishing House, 1982, 104.
18. Crawford, M. L., Phase equilibria in aqueous fluid inclusions (eds. L. S. Hollisterand, M. L. Crawford), Short Course in Fluid Inclusions: Applications to Petrology, Mineralogical Association of Canada, 1981, 3: 157－181.
19. Dubessy, J., Audeoud, D., Wilkins, R., The use of the raman miniroprobe mole in the determination of the electrolytes dissolved in the aqueous phase of fluid inclusions, Chemical Geology, 1982, 37: 137－150.
20. Schrotter, H. W., Raman Scattering Cross Cections in Gases and Liquids, Raman Spectroscopy (Theory and Practice) Section 4, New York, 1979, 4: 31－45.